ACS APPLIED MATERIALS & INTERFACES

Research Article

www.acsami.org

High-Performance Hybrid Buffer Layer Using 1,4,5,8,9,11-Hexaazatriphenylenehexacarbonitrile/Molybdenum Oxide in Inverted Top-Emitting Organic Light-Emitting Diodes

Cheol Hwee Park,[†] Hyun Jun Lee,[†] Ju Hyun Hwang,[†] Kyu Nyun Kim,[†] Yong Sub Shim,[†] Sun-Gyu Jung,[†] Chan Hyuk Park,[†] Young Wook Park,*[,‡] and Byeong-Kwon Ju*[,†]

[†]Display and Nanosystem Laboratory, College of Engineering, Korea University, Seoul 136-713, Republic of Korea

[‡]The Institute for High Technology Materials and Devices, Korea University, Seoul 136-713, Republic of Korea

Supporting Information

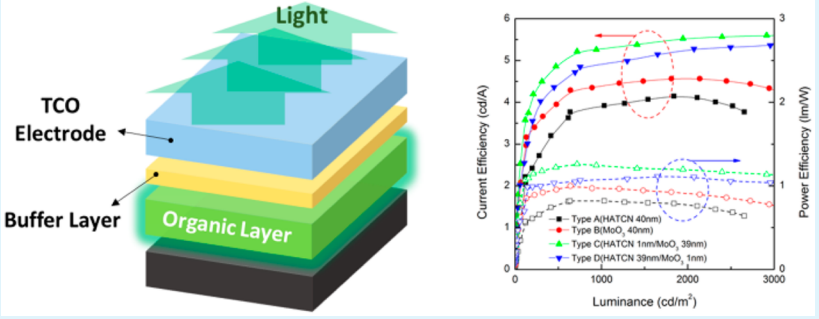

ABSTRACT: A high-performance 1,4,5,8,9,11-hexaazatriphenylenehexacarbonitrile (HATCN)/molybdenum oxide (MoO_3) hybrid buffer layer with high hole-injection efficiency and superior plasma resistance under the sputtering process was developed. The HATCN enhances the hole-injection efficiency, and the MoO_3 effectively protects the underlying organic layers from plasma damage during deposition by sputtering. This improves the characteristics of inverted top-emitting organic light-emitting diodes using a top transparent conductive oxide electrode. The device using the hybrid buffer layer showed the highest electroluminescence characteristics among devices with other buffer layers. The high hole-injection efficiency of HATCN was shown by the *J*–*F* curve of hole-only devices, and the plasma protection performance of MoO_3 was shown by atomic force microscope surface morphology images of the buffer layer film after O_2 plasma treatment.

KEYWORDS: *inverted top-emitting organic light-emitting diodes (ITEOLEDs), buffer Layer, 1,4,5,8,9,11-hexaazatriphenylenehexacarbonitrile (HATCN), molybdenum oxide (MoO_3)*

1. INTRODUCTION

Organic light-emitting diodes (OLEDs) have attracted increasing attention for use in future displays and lighting because of various factors such as flexibility or transparency, low power consumption, and high color purity.[1] Active-matrix OLEDs (AMOLEDs) are already used in commercial products such as mobile cell phones, tablets, and televisions. In AMOLEDs, low-temperature polysilicon (LTPS) is used as the thin-film transistor (TFT) backplanes that underlie the OLED pixels. LTPS is a superior p-type doped TFT with high carrier mobility and stability. However, when large displays are fabricated, LTPS has disadvantages such as nonuniformity and costly fabrication. To avoid the disadvantages of LTPS, many research groups have studied an oxide TFT. Unlike p-type LTPS, oxide TFT backplanes have mainly n-type transistor characteristics.[2−6] Consequently, the inverted OLED structure with the bottom cathode directly connected to the drain line of the n-type TFT is more suitable for AMOLEDs with an oxide TFT than the conventional OLED structure with the top cathode and bottom anode. Using the inverted OLED structure decreases the driving voltage, and the voltage drop that causes image sticking in AMOLEDs with the conventional OLED structure and n-type TFT backplanes is minimized.[7,8]

The top-emitting (TE) structure is suitable for high-efficiency AMOLEDs because it allows the design of a large aperture ratio for high-resolution displays without being affected by the pixel circuits.[9,10] For this reason, the inverted top-emitting OLED (ITEOLED) is the ideal OLED structure in AMOLED displays. The main concerns in fabrication are obtaining a (semi)transparent top anode and a highly reflective bottom cathode and supplying superior carrier injection efficiency to the organic layer. Ag and Al have typically been used for the bottom cathode because they have excellent reflective performance.[10−12] Lithium fluoride (LiF) and cesium

Received: June 8, 2014
Accepted: March 5, 2015
Published: March 11, 2015

ACS Publications © 2015 American Chemical Society

DOI: 10.1021/am5091066
ACS Appl. Mater. Interfaces 2015, 7, 6047−6053

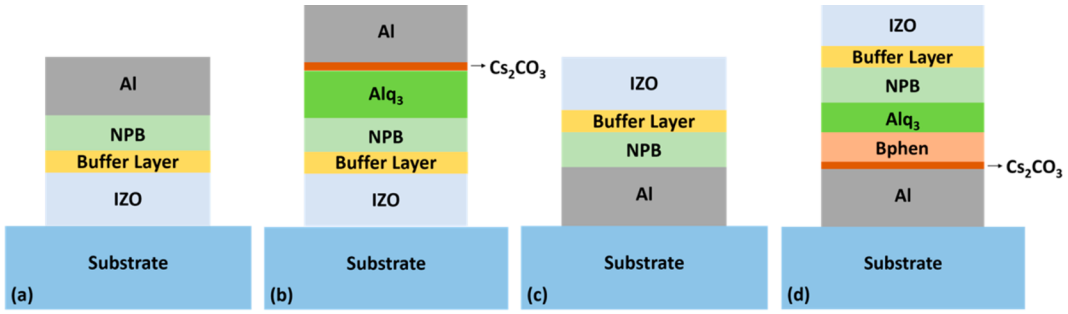

Figure 1. Structure of fabricated devices: (a) hole-only device, (b) BEOLED, (c) inverted hole-only device, (d) ITEOLED.

carbonate (Cs_2CO_3) have been used for the bottom cathode to obtain high electron injection efficiency.[7,10,11] As a (semi)-transparent top electrode, thin transparent metals such as Ag have been used, and as a multilayered electrode, materials such as tungsten oxide (WO_3)/Ag/WO_3, and molybdenum oxide (MoO_3)/Ag/MoO_3 have been used.[7,13,14] Such electrodes and other type of electrodes can form an excellent electrical contact with the organic layers and have a low sheet resistance of less than 10 $\Omega\square^{-1}$ and a high transparency of around 80% in a certain spectral range; however, their transmittances were not as high as those of a transparent conducting oxide (TCO) such as indium tin oxide (ITO), indium zinc oxide (IZO), or aluminum-doped zinc oxide when the entire visible light spectrum was considered.[7,13−16] To achieve high transmittance, TCOs have been used as a transparent top electrode. However, they are usually deposited by a sputtering process under various gas plasmas such as oxygen and argon, and the plasma easily causes critical damage to the organic materials, which thus degrade easily during the plasma deposition process. To prevent degradation of the organic materials during the sputtering process, a stable buffer layer must be additionally formed between the TCO and the organic layers. In addition, high transparency at visible wavelengths and excellent charge injection from the TCO are essential characteristics of the buffer layer in the fabrication of highly efficient ITEOLEDs. Many research groups have introduced various organic and inorganic buffer layer materials such as copper phthalocyanine doped with F_4-TCNQ,[17] 1,4,5,8,9,11-hexaazatriphenylenehexacarbonitrile (HATCN),[18] $Ni(acac)_2$,[19] WO_3,[20] poly(3,4-ethylenedioxythiophene) poly(styrene-sulfonate),[21,22] pentacene,[22,23] 3,4,9,10-perylenetetracarboxylic dianhydride,[24] and 2,9-dimethyl-4,7-diphenyl-1,10-phenanthroline/Li,[25] and MoO_3.[26] Although these buffer layers reported to show a possibility of using as a buffer layer followed by TCO sputtering, and some of them were reported to show a good protection ability (especially WO_3[20] and MoO_3[26]), but there is still an argument of correlation between the plasma damage, protection ability, and injection ability after TCO sputtering deposition. In this work, we demonstrated the HATCN/MoO_3 hybrid type buffer layer having perfect plasma protection ability and high hole-injection ability compared to single buffer layers, and reported the ITEOLEDs utilized by this hybrid buffer layer. HATCN was reported to be plasma damage sustainable[18] and to have 100% injection efficiency,[27] but it was found to suffer from plasma damage during TCO deposition. By using MoO_3 upper layer on HATCN structure hybrid buffer layer, the HATCN enhances the hole-injection efficiency, and the MoO_3 protects the underlying organic layers from plasma damage.

2. EXPERIMENTAL DETAILS

First, the hole-injection performance was measured in "hole-only" devices using the current density versus average applied electric field (*J*−*F*) characteristics, and the plasma protection performance was investigated using the electroluminescence (EL) characteristics of the OLED and a plasma treatment test at the buffer layer. Both the bottom-emitting (BE) and ITE structures were investigated. The results showed that HATCN has superior hole-injection performance compared to MoO_3 at the interface between the sputtered IZO top electrode and the *N*,*N*′-bis(naphthalen-1-yl)-*N*,*N*′-bis(phenyl)-benzidine (NPB) hole transport layer. However, although HATCN has been reported to have high plasma durability and showed better performance in the BEOLED, the HATCN buffer layer devices showed a degraded surface (visible in optical images) and EL characteristics compared to the MoO_3 device in the ITEOLED. Thus, HATCN has a much lower plasma durability than MoO_3. In other words, MoO_3 offers much better plasma protection than HATCN and thus shows much higher current injection in the ITEOLED but not in the BEOLED. Finally, the ITEOLED with the HATCN/MoO_3 hybrid buffer layer exhibits the best performance.

Figure 1 shows the structures of the hole-only devices and OLEDs with BE and TE structures. All the devices were fabricated on chemically cleaned substrates. Eagle XG glass substrates were cleaned in an ultrasonic bath with acetone, methanol, and deionized water for 15 min each. They were then dried in an oven at 120 °C. After the cleaning process, different functional layers were sequentially deposited on the cleaned substrates by thermal evaporation under a vacuum of 10^{-6} Torr. The NPB was used as the hole-transport layer, tris(8-hydroxyquinolinato)-aluminum (Alq_3) was used as the emitting layer and 4,7-diphenyl-1,10-phenanthroline (Bphen) was used as the electron transport layer. Cs_2CO_3 was used as the electron-injection layer, and Al was used as the cathode. As a buffer layer and hole-injection layer, MoO_3 and HATCN were used. The deposition rates of all of the organic materials and metals were 1 and 3 Å/s, respectively. Then, the IZO used as an anode was deposited by radio frequency (RF) magnetron sputtering. All the devices have a 4 × 4 mm active area.

The O_2 plasma treatment for investigation of the plasma protection performance of the buffer layers was performed for 40 s under O_2 filling a 30 mTorr vacuum reactive ion etching chamber. The plasma RF power was 50 W.

The EL and current density−average applied electric field (*J*−*F*) characteristics of the fabricated OLEDs and hole-only devices were measured using a high voltage source measurement unit (Model 237, Keithley Instruments, Inc.) and a spectroradiometer (PR-670 SpectraScan, Photo Research, Inc.). Surface topology images of the buffer layer films on NPB were taken using an atomic force microscope (AFM) (XE-100, Park Systems AFM).

3. RESULTS AND DISCUSSION

In this study, we used four different buffer layers, as summarized in Table 1. Types A, B, C, and D have buffer layers consisting of HATCN (40 nm), MoO_3 (40 nm), HATCN (1 nm)/MoO_3 (39 nm), and HATCN (39 nm)/

DOI: 10.1021/am5091066
ACS Appl. Mater. Interfaces 2015, 7, 6047−6053

Table 1. Types of Buffer Layers

type	buffer layer	
	conventional structure	inverted structure
A	HATCN (40 nm)	HATCN (40 nm)
B	MoO_3 (40 nm)	MoO_3 (40 nm)
C	MoO_3 (39 nm)/HATCN (1 nm)	HATCN (1 nm)/ MoO_3 (39 nm)
D	MoO_3 (1 nm)/HATCN (39 nm)	HATCN (39 nm)/ MoO_3 (1 nm)

MoO_3 (1 nm), respectively, between the NPB hole transport layer and IZO anode. In our approach to a buffer layer with high hole-injection efficiency and plasma protection to improve the OLED performance, we investigated two hole-only devices and two OLEDs for BEOLEDs and four inverted hole-only devices and four OLEDs for ITEOLEDs with various types of buffer layers. The structure of the hole-only device for BEOLEDs (Figure 1a) is IZO (200 nm)/buffer layer (40 nm)/NPB (80 nm)/Al (100 nm); that of the OLEDs for BEOLEDs (Figure 1b) is IZO (200 nm)/buffer layer (40 nm)/NPB (60 nm)/Alq_3 (80 nm)/Cs_2CO_3 (2 nm)/Al (100 nm). The structure of the inverted hole-only device is Al (100 nm)/NPB (80 nm)/buffer layer (40 nm)/IZO (200 nm); that of the OLEDs for ITEOLEDs is Al (100 nm)/Cs_2CO_3 (2 nm)/Bphen (50 nm)/Alq_3 (30 nm)/NPB (60 nm)/buffer layer (40 nm)/IZO (200 nm).

For the hole-only devices and BEOLEDs, we show the hole-injection efficiency of the buffer layers with IZO anode. As shown in Figure 2, the *J*–*F* characteristics of the Type A hole-only device reveal a higher current density than the Type B device at the same electric field (from the ohmic response region of below 200 kV/cm to operational region of over 200 kV/cm). This result indicates that the hole-injection ability and mobility of the HATCN acting as a buffer layer between the IZO and NPB is superior to that of MoO_3. In 2012, So et al. reported the characteristics of two hole-injection materials HATCN and MoO_3; they demonstrated HATCN has higher hole-injection efficiency than MoO_3 as a hole-injection layer between the ITO and NPB.[27] Generally, ITO and IZO have similar work functions, 4.7[28] and 4.77 eV,[29] respectively. Thus, hole-injection ability of HATCN is higher than MoO_3 in based on IZO anode device.

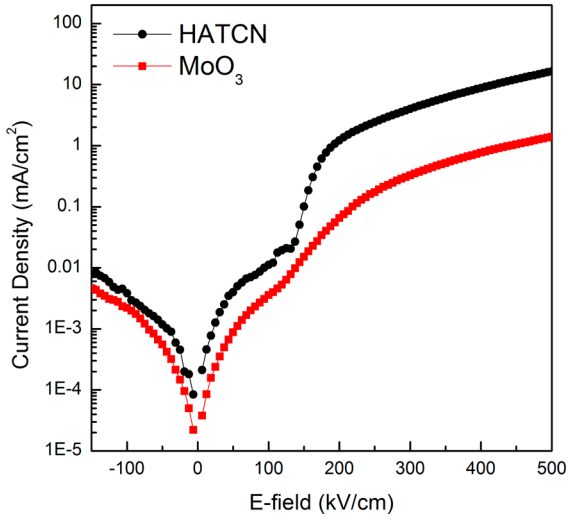

Figure 2. *J*–*F* characteristics of hole-only devices.

Next, to investigate the hole-injection performance of the HATCN and MoO_3 buffer layer in the OLEDs, we performed an additional experiment and obtained the current density–voltage–luminance (*J*–*V*–*L*) and current efficiency–luminance–power efficiency (CE–*L*–PE) characteristics of BEOLEDs with the buffer layer, as shown in Figure 3. Because HATCN has higher hole-injection efficiency than MoO_3, Type A (BEOLEDs with a HATCN buffer layer) has a lower operating voltage and more superior carrier balance with Cs_2CO_3/Al cathode structure than Type B (BEOLEDs with a MoO_3 buffer layer). Thus, BEOLEDs with the HATCN buffer layer show higher current density, luminance, CE, and PE characteristics than those of BEOLEDs with the MoO_3 buffer layer as in Figure 3.

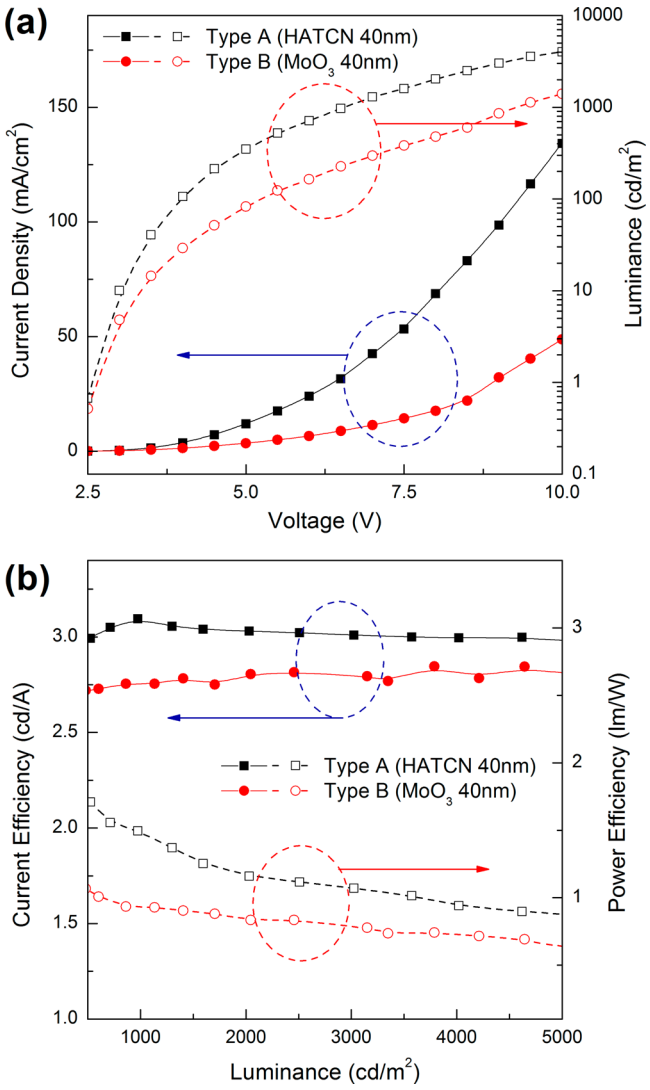

Figure 3. EL characteristics of BEOLEDs. (a) Current density and luminance versus voltage. (b) Current and power efficiency versus luminance.

Although HATCN has higher hole-injection efficiency than MoO_3, it yields different results in the inverted devices. Figures 4 and 5 show the hole-injection performance and electroluminescence characteristics, respectively, of inverted hole-only devices and ITEOLEDs with four different types of buffer layers. The *J*–*F* characteristics of the inverted hole-only devices

DOI: 10.1021/am5091066
ACS Appl. Mater. Interfaces 2015, 7, 6047–6053

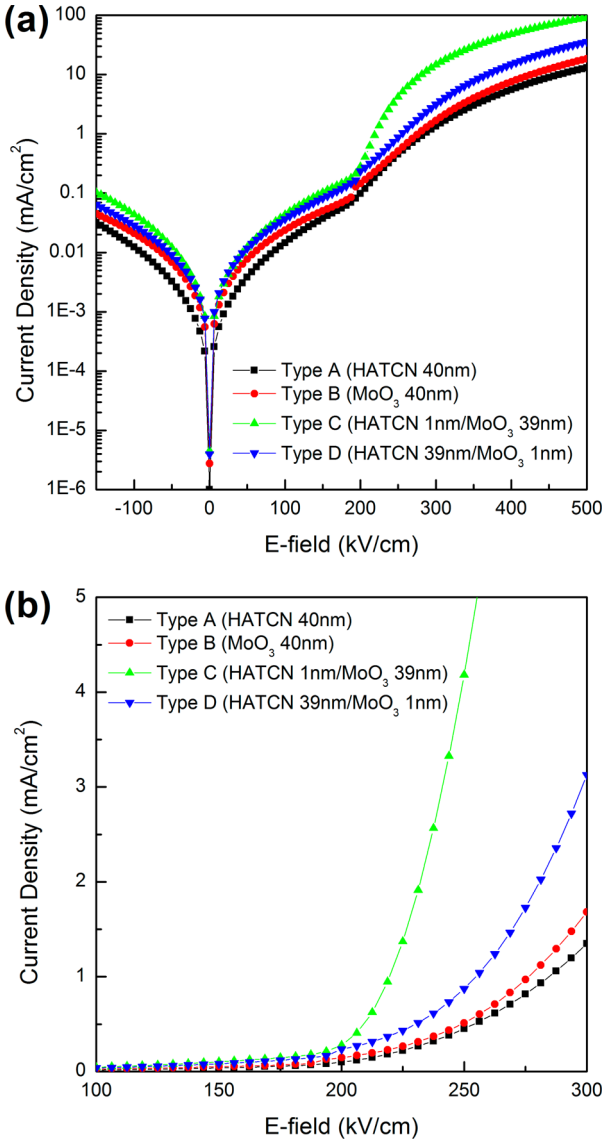

Figure 4. *J*–*F* characteristic of inverted hole-only devices; (a) log scale and (b) linear scale.

are shown in Figure 4. It shows the same order of current density at overall applied electrical field (ohmic behavior region of below 200 kV/cm, operational region of over 200 kV/cm): Type C (HATCN 1 nm/thick MoO_3 39 nm) > Type D (HATCN 39 nm/thin MoO_3 1 nm) > Type B (MoO_3 40 nm) > Type A (HATCN 40 nm). In contrast to the hole-only devices for the BE structure, the *J*–*F* behavior of the inverted hole-only devices differ depending on the buffer layer; the MoO_3 buffer layer (Type B) shows higher current injection than the HATCN buffer layer (Type A). This result indicates that although HATCN has high hole-injection efficiency, it was damaged by plasma during sputtering deposition. Thus, its hole-injection efficiency decreased, and the plasma-stable MoO_3 buffer layer has a higher current density. Although HATCN was reported as a plasma-stable buffer layer in ITEOLEDs,[18] our results show remarkable damage to HATCN by plasma during the sputtering process. For further comparison, a double-layered hybrid buffer layer (HATCN/MoO_3) was tested. HATCN was used to provide hole-injection, and MoO_3 on HATCN was used to provide plasma protection.

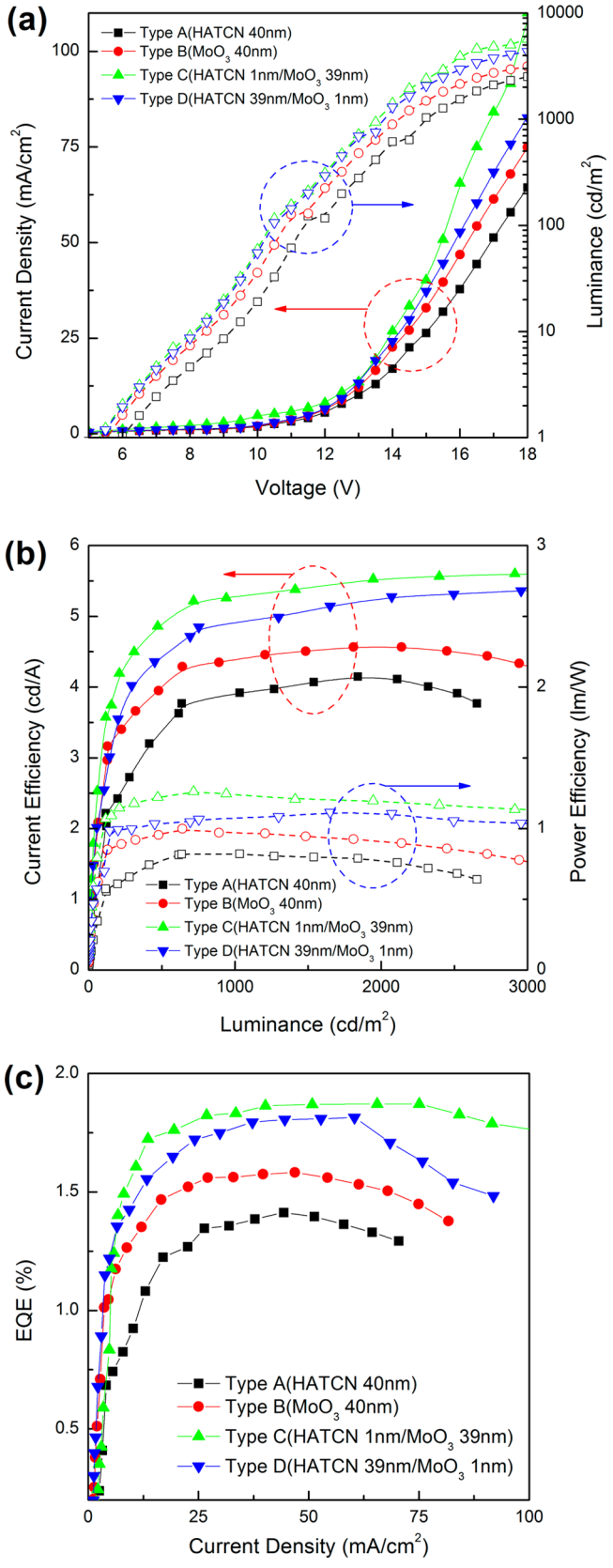

Figure 5. EL characteristics of ITEOLEDs. (a) Current density and luminance versus voltage. (b) Current and power efficiency versus luminance. (c) EQE versus current density.

The hybrid buffer layers, Types C and D, show much higher hole-injection efficiency than the single buffer layers of Types A

DOI: 10.1021/am5091066
ACS Appl. Mater. Interfaces 2015, 7, 6047–6053

and B. Compared to the Type D device [thick HATCN (39 nm)/thin MoO_3 (1 nm)], the Type C inverted hole-only device with thin HATCN (1 nm)/thick MoO_3 (39 nm) shows much higher hole-injection performance. This result indicates that the HATCN in Type C was damaged less than the HATCN in Type D because of the thicker MoO_3; thus, the Type C inverted hole-only device exhibits more efficient current injection than the Type D device. This result for the hybrid buffer layer confirms that the MoO_3 buffer layer is more stable than HATCN under sputtering. The plasma protection performance is also visible in the optical microscope images in Figure S1 (Supporting Information). In addition, the hybrid buffer layer increases the $J-V$ characteristics. This result also contributes to the large increase in the EL efficiency of the ITEOLEDs.

The EL characteristics of ITEOLEDs with different buffer layers are shown in Figure 5 and summarized in Table 2.

Table 2. EL Characteristics of Fabricated ITEOLEDs

type	turn-on voltage (at 1 cd/m^2)	V at 500 cd/m^2	CE (cd/A) at 1000 cd/m^2	PE (lm/W) at 1000 cd/m^2	EQE (%) at 50 mA/cm^2
A	5.98	13.71	3.91	0.82	1.40
B	5.52	13.05	4.41	0.97	1.57
C	5.30	12.56	5.44	1.20	1.87
D	5.35	12.60	4.91	1.07	1.81

According to the preceding experimental results, MoO_3 is more suitable as a plasma protection buffer layer than HATCN, and HATCN outperforms MoO_3 as a hole-injection layer. Thus, the $J-V-L$ characteristic of the ITEOLEDs is similar to those in Figure 4. In Figure 5a, the Type C device shows the highest current density (40.19 mA/cm^2 at 15 V), compared to that of Type A (Type A, 26.35 mA/cm^2 at 15 V; Type B, 32.93 mA/cm^2 at 15 V; Type D, 37.24 mA/cm^2 at 15 V). In addition, Figure 5b,c shows that the Type C device has the highest CE, PE, and external quantum efficiency (EQE): 5.44, 1.2 at 1000 cd/m^2, and 1.87 at 50 mA/cm^2, respectively) than the others (Type A, 3.91, 0.82 at 1000 cd/m^2, and 1.4 at 50 mA/cm^2; Type B, 4.41, 0.97 at 1000 cd/m^2, and 1.57 at 50 mA/cm^2; Type D, 4.91, 1.07 at 1000 cd/m^2, and 1.81 at 50 mA/cm^2, respectively). These results show that the hybrid buffer layer type C has superior plasma protection ability and hole-injection efficiency in ITEOLED with IZO top electrode and ITEOLEDs with hybrid buffer layer have more powerful efficiency than devices with single buffer layer.

To confirm the stability of the various buffer layers under sputtering, we investigated surface topography images of the deposited buffer layer on the NPB using an AFM (before and after O_2 plasma treatment). For the comparison, two different structures were used [NPB (40 nm)/HATCN (40 nm) and NPB (40 nm)/MoO_3 (40 nm)], and images of these structures' topologies are shown in Figure 6. Figure 6a shows bare NPB/HATCN, Figure 6b shows bare NPB/MoO_3, Figure 6c shows the NPB/HATCN after plasma treatment, and Figure 6d shows the NPB/MoO_3 after plasma treatment. The topology changes when the buffer layer materials are deposited onto the NPB film. The surfaces of the HATCN and MoO_3 have a peak-to-valley roughness (R_{pv}) of 16.67 and 6.81 nm, respectively. After O_2 plasma treatment for 40 s, the HATCN surface became rougher, with an R_{pv} value of 34.83 nm, whereas the MoO_3 surface became smoother, with an R_{pv} value of 3.42 nm. In addition, the root-mean-square roughness (R_q) of the HATCN film increased from 2.13 to 3.60 nm; on the other hand, the R_q value of the MoO_3 film decreased from 0.63 to 0.36 nm after O_2 plasma treatment. Compared with HATCN, the surface roughness of MoO_3 changed less, and the surface became smoother after O_2 plasma treatment. This result indicates that MoO_3 has a higher plasma resistance under O_2 plasma treatment than HATCN when used as a buffer layer, which supports the experimental results in Figures 4 and 5a. The results of a multilateral roughness analysis of all the samples (R_{pv}, R_q, and the average roughness (R_a)) are summarized in Table 3.

Table 3. Morphological Characteristics of Thin Films from AFM Measurements before and after O_2 Plasma Treatment

	R_{pv} (nm)[a]	R_q (nm)[b]	R_a (nm)[c]
NPB/HATCN (before O_2 plasma)	16.67	2.13	1.67
NPB/HATCN (after O_2 plasma)	34.83	3.60	2.78
NPB/MoO_3 (before O_2 plasma)	6.81	0.63	0.49
NPB/MoO_3 (after O_2 plasma)	3.42	0.36	0.28

[a]Peak-to-valley roughness. [b]Root mean square roughness. [c]Average roughness.

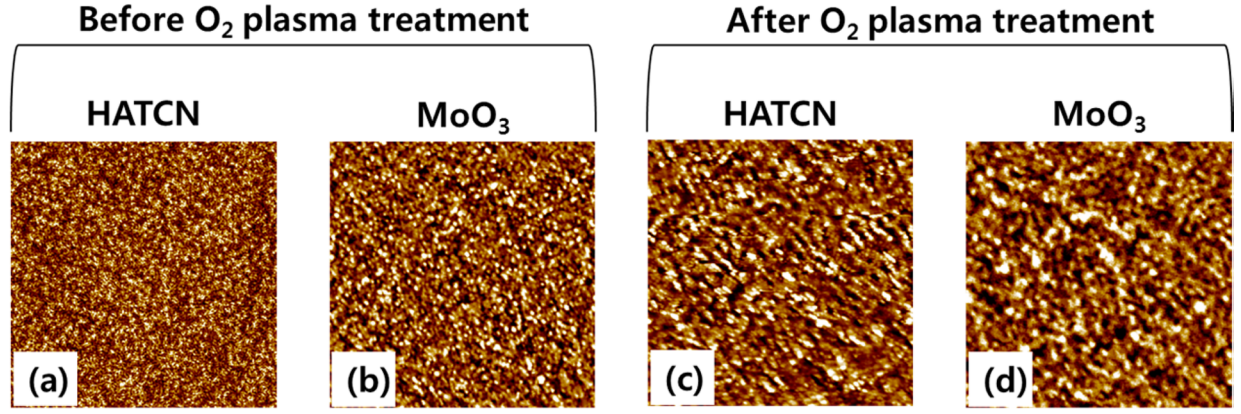

Figure 6. Surface topology images of (a) 40 nm thick HATCN grown on the NPB (40 nm)/glass substrate and (b) 40 nm thick MoO_3 grown on the NPB (40 nm)/glass substrate measured using an AFM before O_2 plasma treatment and topology images of (c) HATCN and (d) MoO_3 films after O_2 plasma treatment.

DOI: 10.1021/am5091066
ACS Appl. Mater. Interfaces 2015, 7, 6047−6053

Next, we research the lifetime of ITEOLEDs with buffer layers. Figure S3 (Supporting Information) shows the lifetime of ITEOLEDs. Device 3 (HATCN 1 nm/MoO_3 39 nm/IZO 100 nm) has +492%, +149%, and +443% longer LT50 lifetime than Device 1 (HATCN 40 nm/IZO 100 nm), Device 2 (MoO_3 40 nm/IZO 100 nm) and Device 4 (HATCN 1 nm/MoO_3 39 nm/Ag 30 nm), respectively. This result indicates the hybrid buffer layer type C (thin HATCN/thick MoO3) has not only perfect protection ability from the gas plasma but also stability.

4. CONCLUSION

In summary, we successfully demonstrated a high-performance hybrid buffer layer between a hole-transport layer (NPB) and top electrode (IZO) for a high-efficiency ITEOLED. Although HATCN has been reported as a highly plasma-durable buffer layer for ITEOLEDs, it still showed remarkable degradation; however, the hybrid buffer layer demonstrated here (thin HATCN/thick MoO_3) shows high plasma durability and highly improved current injection characteristics. The two buffer layer materials, HATCN and MoO_3, each have an important role. HATCN has high hole-injection efficiency and can effectively inject holes to the hole-transport layer from the anode. MoO_3 has high plasma resistance and can be used to fabricate OLEDs with a TCO top electrode deposited by sputtering. The plasma durability and degradation characteristics of the buffer layers were confirmed well by AFM measurements and a systematic analysis of the device characteristics. And the lifetime of ITEOLEDs shows that the ITEOLED with the hybrid type buffer layer is more stable than the single buffer layer device and the thin Ag top electrode device. These results demonstrate that the HATCN/MoO_3 hybrid buffer layer has excellent hole-injection and plasma protection performance. In addition, we expect that the hybrid buffer layer developed in this study can be directly adapted to a high-performance AMOLED display with a TCO top electrode based on an oxide TFT.

■ ASSOCIATED CONTENT

Supporting Information

Optical microscope images of ITEOLEDs after sputtering process, photographs of buffer layers after plasma treatment, lifetime measurement of ITEOLEDs, and SIMS analysis. This material is available free of charge via the Internet at http://pubs.acs.org.

■ AUTHOR INFORMATION

Corresponding Authors

*E-mail: zerook@korea.ac.kr,
*E-mail: bkju@korea.ac.kr.

Notes

The authors declare no competing financial interest.

■ ACKNOWLEDGMENTS

This research was supported by the Basic Science Research Program through the National Research Foundation of Korea (NRF), funded by the Ministry of Education, Science and Technology (2012R1A6A3A04039396), an NRF grant funded by the Korean government (MSIP) (CAFDC 4−2, NRF 2007−0056090), and the Industry Technology R&D program of MOTIE/KEIT (10048317, development of red and blue OLEDs with external quantum efficiency over 20% using delayed fluorescent materials). The authors thank the staff of KBSI for technical assistance.

■ REFERENCES

(1) Reineke, S.; Lindner, F.; Schwartz, G.; Seidler, N.; Walzer, K.; Lüssem, B.; Leo, K. White Organic Light-Emitting Diodes with Fluorescent Tube Efficiency. *Nature* **2009**, *459*, 234.
(2) Stewart, M.; Howell, R. S.; Pires, L.; Hatalis, M. K. Polysilicon TFT Technology for Active Matrix OLED Displays. *IEEE Trans. Electron Devices* **2001**, *48*, 845−851.
(3) Yun, C.; Cho, H.; Kang, H.; Lee, Y. M.; Park, Y.; Yoo, S. Electron Injection via Pentacene Thin Films for Efficient Inverted Organic Light-Emitting Diodes. *Appl. Phys. Lett.* **2009**, *95*, 053301.
(4) Lee, H.; Park, I.; Kwak, J.; Yoon, D. Y.; Lee, C. Improvement of Electron Injection in Inverted Bottom-Emission Blue Phosphorescent Organic Light Emitting Diodes using Zinc Oxide Nanoparticles. *Appl. Phys. Lett.* **2010**, *96*, 153306.
(5) Chu, T.-Y.; Chen, J.-F.; Chen, S.-Y.; Chen, C.-J.; Chen, C. H. Highly Efficient and Stable Inverted Bottom-Emission Organic Light Emitting Devices. *Appl. Phys. Lett.* **2006**, *89*, 053503.
(6) He, Y.; Hattori, R.; Kanicki, J. Improved a-Si:H TFT Pixel Electrode Circuits for Active-Matrix Organic Light Emitting Displays. *IEEE Trans. Electron Devices* **2001**, *48*, 1322−1325.
(7) Zhang, X.-W.; Xu, J.-W.; Xu, H.-R.; Lin, H.-P.; Li, J.; Jiang, X.-Y.; Zhang, Z.-L. Improving Electron Injection and Microcavity Effect for Constructing Highly Efficient Inverted Top-Emitting Organic Light-Emitting Diode. *Opt. Laser. Technol.* **2013**, *45*, 181−184.
(8) Lee, H.; Kang, C. M.; Park, M.; Kwak, J.; Lee, C. Improved Efficiency of Inverted Organic Light-Emitting Diodes using Tin Dioxide Nanoparticles as an Electron Injection Layer. *ACS Appl. Mater. Interfaces* **2013**, *5*, 1977−1981.
(9) Lim, J. T.; Park, J. W.; Yeom, G. Y. Interfacial Electronic Structure of Molybdenum Oxide on the Fullerene Layer, a Potential Hole-Injecting Layer in Inverted Top-Emitting Organic Light-Emitting Diodes. *Curr. Appl. Phys.* **2013**, *13*, 1037−1041.
(10) Knauer, K. A.; Najafabadi, E.; Haske, W.; Gaj, M. P.; Davis, K. C.; Fuentes-Hernandez, C.; Carrasco, U.; Kippelen, B. Stacked Inverted Top-Emitting Green Electrophosphorescent Organic Light-Emitting Diodes on Glass and Flexible Glass Substrates. *Org. Electron* **2013**, *14*, 2418−2423.
(11) Najafabadi, E.; Knauer, K. A.; Haske, W.; Kippelen, B. High-Performance Inverted Top-Emitting Green Electrophosphorescent Organic Light-Emitting Diodes with a Modified Top Ag Anode. *Org. Electron.* **2013**, *14*, 1271−1275.
(12) Thomschke, M.; Hofmann, S.; Olthof, S.; Anderson, M.; Kleemann, H.; Schober, M.; Lüssem, B.; Leo, K. Improvement of Voltage and Charge Balance in Inverted Top-Emitting Organic Electroluminescent Diodes Comprising Doped Transport Layers by Thermal Annealing. *Appl. Phys. Lett.* **2011**, *98*, 083304.
(13) Yook, K. S.; Jeon, S. O.; Joo, C. W.; Lee, J. Y. Transparent Organic Light Emitting Diodes using a Multilayer Oxide as a low Resistance Transparent Cathode. *Appl. Phys. Lett.* **2008**, *93*, 013301.
(14) Yambem, S. D.; Ullah, M.; Tandy, K.; Burn, P. L.; Namdas, E. B. ITO-Free Top Emitting Organic Light Emitting Diodes with Enhanced Light Out-Coupling. *Laser. Photonics. Rev.* **2014**, *8*, 165−171.
(15) Han, S.; Feng, X.; Lu, Z. H.; Johnson, D.; Wood, R. Transparent-Cathode for Top-Emission Organic Light-Emitting Diodes. *Appl. Phys. Lett.* **2003**, *82*, 2715.
(16) Lee, J.; Hofmann, S.; Furno, M.; Thomschke, M.; Kim, Y. H.; Lüssem, B.; Leo, K. Influence of Organic Capping Layers on the Performance of Transparent Organic Light-Emitting Diodes. *Opt. Lett.* **2011**, *36*, 1443−1445.
(17) Pfeiffer, M.; Forrest, S. R.; Zhou, X.; Leo, K. A Low Drive Voltage, Transparent, Metal-Free n−i−p Electrophosphorescent Light Emitting Diode. *Org. Electron* **2003**, *4*, 21−26.
(18) Lee, J.-H.; Lee, S.; Kim, J.-B.; Jang, J.; Kim, J.-J. A High Performance Transparent Inverted Organic Light Emitting Diode with

DOI: 10.1021/am5091066
ACS Appl. Mater. Interfaces 2015, 7, 6047−6053

1,4,5,8,9,11-Hexaazatriphenylenehexa-carbonitrile as an Organic Buffer Layer. *J. Mater. Chem.* **2012**, *22*, 15262.
(19) Yamamori, A.; Hayashi, S.; Koyama, T.; Taniguchi, Y. Transparent Organic Light-Emitting Diodes using Metal Acethylacetonate Complexes as an Electron Injective Buffer Layer. *Appl. Phys. Lett.* **2001**, *78*, 3343.
(20) Meyer, J.; Winkler, T.; Hamwi, S.; Schmale, S.; Johannes, H.-H.; Weimann, T.; Hinze, P.; Kowalsky, W.; Riedl, T. Transparent Inverted Organic Light-Emitting Diodes with a Tungsten Oxide Buffer Layer. *Adv. Mater.* **2008**, *20*, 3839−3843.
(21) Görrn, P.; Sander, M.; Meyer, J.; Kröger, M.; Becker, E.; Johannes, H. H.; Kowalsky, W.; Riedl, T. Towards See-Through Displays: Fully Transparent Thin-Film Transistors Driving Transparent Organic Light-Emitting Diodes. *Adv. Mater.* **2006**, *18*, 738−741.
(22) Dobbertin, T.; Werner, O.; Meyer, J.; Kammoun, A.; Schneider, D.; Riedl, T.; Becker, E.; Johannes, H. H.; Kowalsky, W. Inverted Hybrid Organic Light-Emitting Device with Polyethylene Dioxythiophene-Polystyrene Sulfonate as an Anode Buffer Layer. *Appl. Phys. Lett.* **2003**, *83*, 5071.
(23) Dobbertin, T.; Kroeger, M.; Heithecker, D.; Schneider, D.; Metzdorf, D.; Neuner, H.; Becker, E.; Johannes, H. H.; Kowalsky, W. Inverted Top-Emitting Organic Light-Emitting Diodes using Sputter-Deposited Anodes. *Appl. Phys. Lett.* **2003**, *82*, 284.
(24) Bulović, V.; Tian, P.; Burrows, P. E.; Gokhale, M. R.; Forrest, S. R.; Thompson, M. E. A Surface-Emitting Vacuum-Deposited Organic Light Emitting Device. *Appl. Phys. Lett.* **1997**, *70*, 2954−2956.
(25) Parthasarathy, G.; Adachi, C.; Burrows, P. E.; Forrest, S. R. High-Efficiency Transparent Organic Light-Emitting Devices. *Appl. Phys. Lett.* **2000**, *76*, 2128.
(26) Schmidt, H.; Flügge, H.; Winkler, T.; Bülow, T.; Riedl, T.; Kowalsky, W. Efficient Semitransparent Inverted Organic Solar Cells with Indium Tin Oxide Top Electrode. *Appl. Phys. Lett.* **2009**, *94*, 243302.
(27) Small, C. E.; Tsang, S.-W.; Kido, J.; So, S. K.; So, F. Origin of Enhanced Hole Injection in Inverted Organic Devices with Electron Accepting Interlayer. *Adv. Funct. Mater.* **2012**, *22*, 3261−3266.
(28) Zhou, Y.; Shim, J. W.; Fuentes-Hernandez, C.; Sharma, A.; Knauer, K. A.; Giordano, A. J.; Marder, S. R.; Kippelen, B. Direct Correlation between Work Function of Indium-Tin-Oxide Electrodes and Solar Cell Performance Influenced by Ultraviolet Irradiation and Air Exposure. *Phys. Chem. Chem. Phys.* **2012**, *14*, 12014−12021.
(29) Park, J. H.; Lee, S. J.; Lee, T. I.; Kim, J. H.; Kim, C.-H.; Chae, G. S.; Ham, M.-H.; Baik, H. K.; Myoung, J.-M. All-Solution-Processed, Transparent Thin-Film Transistor based on Metal Oxides and Single-Walled Carbon Nanotubes. *J. Mater. Chem. C* **2013**, *1*, 1840−1845.

DOI: 10.1021/am5091066
ACS Appl. Mater. Interfaces 2015, 7, 6047−6053